Constant-Q wavelet estimation via a Gabor spectral model

J. P. Grossman (Geology and Geophysics), G. F. Margrave (Geology and Geophysics), M. P. Lamoureux (Mathematics and Statistics), and R. Aggarwala (Mathematics and Statistics) - University of Calgary

CSEG Geophysics 2002

Summary

As a seismic wave propagates through the earth, its amplitude attenuates over time and frequency due to microscopic processes such as internal friction. Thus, the earth is an anelastic medium; on the other hand, Hooke's law, which is normally used in the derivation of the wave equation, applies only to perfectly elastic media. Despite this fact, attenuation can be modeled macroscopically over typical seismic bandwidths via an exponential amplitude decay in both time and frequency, at a rate determined by a dimensionless quantity, Q. Current seismic deconvolution methods, based on the stationary convolutional model, attempt to estimate and filter out the embedded causal wavelet. We present a nonstationary seismic model, expressed in the time-frequency Gabor domain, in which (1) the embedded causal wavelet is represented as the product of a stationary seismic signature with a nonstationary exponential decay; and (2) a nonstationary impulse response for the earth is tractable. By least squares fitting our model to the Gabor-transformed seismic trace, we determine a unique Q-value and an estimate of the seismic signature, and thus an estimate of the nonstationary causal wavelet. Using these estimates to obtain a smoothed version of the seismic trace in the time-frequency domain, a least squares nonstationary minimum phase deconvolution filter is constructed. The preliminary results, coded in MATLAB, are very promising.

Introduction

This paper is concerned with the application of Gabor theory to the modelling, analysis, and subsequent deconvolution of a non-stationary, constant-Q-attenuated seismic signal. In a broader context, Gabor deconvolution is discussed by Margrave and Lamoureux (2002). The Gabor theory sets the stage for non-stationary analysis of a signal, "in which time and frequency play symmetrical parts, and which contains 'time analysis' and 'frequency analysis' as special cases." (Gabor, 1946) Our experience with sound, as in speech or music, demands a mathematical description addressing time and frequency analysis on equal footings. The human ear, much like a hydrophone, combined with the brain's processing capabilities, interprets bandlimited acoustic amplitude information as temporally localized packets of spectral information. Conversely, in following a musical score, a musician transforms a time-frequency representation of a signal into temporally varying acoustic amplitude data.

The Fourier theory is an idealization: it fails to capture our intuition that "frequency content" changes with time. "The reason is that the Fourier-integral method considers phenomena in an infinite interval, …and this is very far from our everyday point of view."(Gabor, 1946) These fundamental observations suggest that we ought to be modelling the localized time and frequency characteristics of a seismic signal simultaneously; and it is the milestone theory of Gabor that provides us with appropriate tools.

We first outline a derivation, to first order, of a time-variant spectral model for the Gabor transform of a constant-Q-attenuated seismic trace. Remarkably, in addition to being intuitively plausible, this model generalizes the familiar convolutional model (as described in Sheriff and Geldart, 1982, for example). Next, the model is fitted to the data in the least squares sense. This process provides estimates for both Q and the stationary part of the wavelet, and thus an estimate of the nonstationary, Q-attenuated wavelet. The theory is then applied in an algorithm for the deconvolution of a Q-attenuated synthetic seismogram, and the preliminary results are discussed.

Theory

A time-variant Gabor spectral model. Let $r(t)$ be a reflectivity, $w(t)$ a stationary source signature, and $\alpha(t,f)$ the time-frequency symbol of a constant Q operator. Specifically for the latter

$$\alpha(t,f) = e^{-\pi f t/Q - iH(\pi f t/Q)}, \qquad (1)$$

where H is the Hilbert transform. The stationary source signature, in this context, is a wavelet whose time-frequency decomposition is equivalent to its Fourier transform, which depends only on frequency. An assumption is that this Fourier transform, $\hat{w}(f)$, is smooth; by definition, $\alpha(t,f)$ is also reasonably smooth.

A nonstationary synthetic trace, $s(t)$, can be constructed by nonstationary convolution (Margrave, 1998) of the Q operator with the reflectivity, followed by stationary convolution with the source signature. Using the mixed domain form of nonstationary convolution (Margrave, 1998) gives

$$\hat{s}(f) = \hat{w}(f) \int_{-\infty}^{\infty} \alpha(t,f) r(t) e^{-2\pi i f t} dt, \qquad (2)$$

where the hat denotes the Fourier transform. Thus

$$s(t) = \int_{-\infty}^{\infty} \hat{w}(f) \left[\int_{-\infty}^{\infty} \alpha(u,f) r(u) e^{-2\pi i f u} du \right] e^{2\pi i f t} df$$

$$= \iint \hat{w}(f) \alpha(u,f) r(u) e^{2\pi i f [t-u]} df du. \qquad (3)$$

Now, the Gabor transform of $s(t)$ is defined as

$$\overset{)}{s}(\tau,f) = \int_{-\infty}^{\infty} s(t) g(t-\tau) e^{-2\pi i f t} dt \qquad (4)$$

where $g(t)$ is the Gabor analysis window, usually a Gaussian (see Feichtinger and Strohmer, 1998, for more on Gabor analysis). Margrave and Lamoureux (2002) showed that the Gabor transform of $s(t)$ can be factorized, to first order, as

$$\overset{)}{s}(\tau,v) = \hat{w}(v) \alpha(\tau,v) \overset{)}{r}(\tau,v). \qquad (5)$$

Discussion of the problem. To first order, then, our Gabor-spectral model is given by equation (5). The problem is simplified by considering only the magnitudes of both sides of (5), namely

$$\left| \overset{)}{s}(\tau,v) \right| = \left| \hat{w}(v) \right| \left| \alpha(\tau,v) \right| \left| \overset{)}{r}(\tau,v) \right|. \qquad (6)$$

We assume that the Gabor transform of the reflectivity is "white", with a mean of unity. Precisely what is meant here by "white" is not easily defined but, intuitively, we mean that $\left| \hat{w}(v) \right| \left| \alpha(\tau,v) \right|$ provides the general spectral shape, while the Gabor spectrum of the reflectivity provides only detail. Thus, we drop the $\left| \overset{)}{r}(\tau,v) \right|$ term from equation (17) and seek a trace model as

$$S(\tau,v) = W(v) e^{-\pi v \tau/Q}, \qquad (7)$$

where $S = \left| \overset{)}{s} \right|$, $W = \left| \hat{w} \right|$, and $e^{-\pi v \tau/Q} = \alpha(\tau,v)$. The equality in (7) is interpreted in the least-squares sense, meaning that a residual error with minimized L^2-norm is assumed. This residual error represents the random ambient noise and the Gabor transform of the reflectivity. A further simplification is obtained by considering the logarithm of both sides of (7), which effectively removes the exponential term:

$$\ln S(\tau,v) = \ln[W(v)] - \pi \tau v/Q. \qquad (8)$$

Once $\left| \hat{w}(v) \right|$ and $\left| \alpha(\tau,v) \right|$ are estimated, their product represents a smoothed version of the Gabor transform of the seismic trace, and it is then a straightforward matter to design a nonstationary, minimum-phase, deconvolution filter.

Solution of the least squares problem. We first ft minimize the function $\alpha = \alpha(W,Q)$ given by

$$\alpha(W,Q) = \iint \left(\ln \frac{S(\tau,v)}{W(v)} + \frac{\pi\tau v}{Q} \right)^2 d\tau dv, \qquad (9)$$

with respect to Q. Equation (9) expresses the square of the L^2-norm of the difference between both sides of (8). The domain of integration is finite since seismic data are bandlimited and of finite duration.

The region of integration, Ω must be selected to encompass only the numerically significant part of the time-variant spectrum of the signal, to avoid large errors due to division by excessively small numbers. For numerical implementations, it is convenient to consider integrals over rectangular domains. All of this can be accomplished by introducing a characteristic weighting function, χ_Ω:

$$\chi_\Omega(\tau,v) = \begin{cases} 1 \text{ if } (\tau,v) \in \Omega \\ 0 \text{ if } (\tau,v) \notin \Omega \end{cases} \qquad (10)$$

as a factor in the integrand. For example,

$$\int_\Omega f(\tau,v) d\tau dv = \int_{v_0}^{v_1} \int_{\tau_0}^{\tau_1} f(\tau,v) \chi_\Omega(\tau,v) d\tau dv, \qquad (11)$$

where *f* is any integrand with numerically stable support Ω, and Ω is contained in the rectangle $[\tau_0,\tau_1] \times [v_0,v_1]$. Any positive weighting function can be substituted for χ_Ω at the discretion of the processor; but it should decay to zero in a smooth way to avoid spectral ringing.

We will assume that an appropriate region Ω (or weighting function) has been selected. Then expression (9) can be written as

$$\alpha(W,Q) = \int_\Omega \left(\ln \frac{S(\tau,v)}{W(v)} + \frac{\pi\tau v}{Q} \right)^2 d\tau dv, \qquad (12)$$

which can be computed according to (11). Minimizing (12) with respect to Q amounts to solving the following equation for Q:

$$0 = \frac{\partial \alpha}{\partial Q} = 2\int_\Omega \left(\ln \frac{S(\tau,v)}{W(v)} + \frac{\pi\tau v}{Q} \right) \left(-\frac{\pi\tau v}{Q^2} \right) d\tau dv. \qquad (13)$$

Straightforward calculations lead to the finite value:

$$Q = \pi \frac{\int_\Omega \tau^2 v^2 d\tau dv}{\int_\Omega \tau v \ln \frac{W(v)}{S(\tau,v)} d\tau dv}. \qquad (14)$$

Since (14) expresses Q in terms of the unknown source signature, $W(v)$, a second expression is required. We seek an optimal function, $W(v)$, using the calculus of variations (see e.g., Marion and Thornton, 1988). Write $s = \ln S$ and $w = \ln W$, and consider an arbitrary variation, $\delta w = \delta w(v)$. Incrementing the unknown function $w(v)$ by $\delta w(v)$, expression (9) becomes

$$\alpha(w+\delta w,Q) = \int_\Omega \left(s(\tau,v) - w(v) - \delta w(v) + \frac{\pi\tau v}{Q} \right)^2 d\tau dv \text{ , or} \qquad (15)$$

$$\alpha(w+\delta w,Q) = \alpha(w,Q) - 2\int_\Omega \left(s(\tau,v) - w(v) + \frac{\pi\tau v}{Q} \right) \delta w(v) d\tau dv \\ + \int_\Omega [\delta w(v)]^2 d\tau dv. \qquad (16)$$

Notice that if we can determine a function $w(v)$ such that the middle term in (16) vanishes, this same function will minimize $\alpha(w,Q)$ with respect to w. This reduces the problem to solving

$$\int_\Omega \left(s(\tau,v) - w(v) + \frac{\pi\tau v}{Q} \right) \delta w(v) d\tau dv = 0 \qquad (17)$$

for $w(v)$. Since $\delta w(v)$ is independent of the time, we have

$$\int_{v_0}^{v_1} \left\{ \int_{\tau_0}^{\tau_1} s(\tau,v) \chi_\Omega(\tau,v) d\tau - \right. \\ \left. w(v) \int_{\tau_0}^{\tau_1} \chi_\Omega(\tau,v) d\tau + \frac{\pi v}{Q} \int_{\tau_0}^{\tau_1} \tau \chi_\Omega(\tau,v) d\tau \right\} \delta w(v) dv = 0. \qquad (18)$$

The v-integral vanishes for all variations $\delta w(v)$, so it follows from the calculus of variations that the function of v inside the braces must vanish. This leads to

$$w(v) = \frac{\int_{\tau_0}^{\tau_1} s(\tau,v) \chi_\Omega(\tau,v) d\tau}{\int_{\tau_0}^{\tau_1} \chi_\Omega(\tau,v) d\tau} + \frac{\pi v}{Q} \frac{\int_{\tau_0}^{\tau_1} \tau \chi_\Omega(\tau,v) d\tau}{\int_{\tau_0}^{\tau_1} \chi_\Omega(\tau,v) d\tau}. \qquad (19)$$

Converting back to the logarithmic notation, we arrive at

$$W(v) = \exp \left\{ \frac{\int_{\tau_0}^{\tau_1} \ln[S(\tau,v)] \chi_\Omega(\tau,v) d\tau}{\int_{\tau_0}^{\tau_1} \chi_\Omega(\tau,v) d\tau} + \frac{\pi v}{Q} \frac{\int_{\tau_0}^{\tau_1} \tau \chi_\Omega(\tau,v) d\tau}{\int_{\tau_0}^{\tau_1} \chi_\Omega(\tau,v) d\tau} \right\}. \qquad (20)$$

The first term in the exponential is the time average of $\ln S(\tau,v)$, while the second term is linear in frequency and proportional to the average time for each frequency. Using a bar to denote the time average, (20) can be written more compactly as

$$W(v) = \exp \left\{ \overline{[\ln S]}(v) + \frac{\pi v}{Q} \bar{\tau}(v) \right\}. \qquad (21)$$

Substitution of (21) into the expression (14) for Q yields

$$Q = \pi \frac{\int_\Omega \tau^2 v^2 d\tau dv}{\int_\Omega \tau v \left[\overline{[\ln S]}(v) + \frac{\pi v}{Q} \bar{\tau}(v) - \ln S(\tau,v) \right] d\tau dv}. \qquad (22)$$

Finally, solving for Q leads to

$$Q = \pi \frac{\int_\Omega \tau v^2 [\tau - \bar{\tau}(v)] d\tau dv}{\int_\Omega \tau v \left[\overline{[\ln S]}(v) - \ln S(\tau,v) \right] d\tau dv}. \qquad (23)$$

Synthetic example

MATLAB functions from the CREWES toolboxes were used extensively in developing the code to generate the least-squares estimates (23) and (21) of Q and $W(v)$, and to perform a Gabor deconvolution. Figure 1 displays a pseudo-random reflectivity and a nonstationary synthetic trace. The synthetic was built by applying a Q operator to the reflectivity, followed by convolution with a 20 Hz minimum phase source signature. The reflectivity has a duration of one second, with a sampling interval of 0.002 seconds.

Figure 2 displays the magnitude of the Gabor transform of the reflectivity. The sample points in the time direction (row number) correspond to successive translations by 0.01 seconds of Gaussian window centers. These Gaussian windows have the property that their sum is approximately equal to one over the duration of the synthetic trace, and their half-width (0.1 seconds) has been selected such that this criterion is met. Each row is computed as the discrete Fourier transform of the windowed trace that is centered at the corresponding offset time. Each sequence of coherent peaks, for instance those at about 1 second, corresponds to a zone of high amplitude in the reflectivity of Figure 1.

The magnitude of the Gabor transform of the synthetic trace is depicted in Figure 3. Since the Q-operator represents an exponential decay surface in time and frequency, its logarithm forms a surface whose contours are hyperbolae, decaying in magnitude according to the product of the time and frequency values. This explains the general decay pattern from the top left toward the bottom right in Figure 3. There is a progressive loss of bandwidth and mean amplitude over time.

Figure 4 displays a weighting function, designed to match the decay pattern of the data, to eliminate data falling below machine precision. This filter was used in the calculation of the integrals in equations (23) and (21) in the manner illustrated in equation (11). This produced an estimated Q value of 28.3, marginally greater than the correct value of 25, and the estimated source signature, whose smoothed Fourier spectrum is plotted with that of the original source signature in Figure 5. Smoothing of this wavelet spectrum, by convolution with a boxcar, was applied to remove small oscillations inherited from the reflectivity.

Figure 6 displays the magnitude of the least-squares model of the data, calculated as

$$\left| w(v) \right|_{est} e^{-\pi v \tau / Q_{est}} \ , \tag{24}$$

where the subscript *est* refers to the least-squares estimates. As expected, the amplitude decays smoothly, and resembles a smeared version of the display in Figure 3. Thus, we refer to this least-squares model as a smoothed representation of the data. The deconvolution operator is approximately the pointwise inverse of (24), combined with the associated nonstationary minimum-phase spectrum. Here, a small positive function, called a stability factor, was added prior to inversion to prevent division by small numbers.

Cross sections of the input and least-squares-modelled Gabor spectra at time t = 0.5s, plotted in decibels, appear in Figure 7. The plot illustrates the effect of the stability factor, which causes the model to deviate from the synthetic data above about 80Hz. Mathematically, the exponential constant-Q operator should decay exponentially over all frequencies, but the plot shows that this is only achieved along the linear trend from about 20Hz to 75Hz. In our noise-free simulation, this is because of limited precision in the calculations; however, increased numerical precision would only mask the real problem of limited precision in seismic recordings.

Figure 8 shows the spectra of the original reflectivity and the Gabor deconvolution result. Whitening has been limited to below 125Hz – half of Nyquist, by a stationary bandpass filter. The two spectra agree quite well over the whitened band. Ultimately, the precision problem mentioned in the previous paragraph limits the degree of whitening that can be achieved. Since the contours of the constant-Q operator are the hyperbolae, $\tau v = $ constant, the maximum possible whitening will be time-variant.

Figure 9 compares the original reflectivity with the least-squares Gabor deconvolution result. The reflector locations are correlated very well, although the amplitudes are slightly mismatched. Figure 10 compares this deconvolution result with a bandlimited version of the original reflectivity (DC to half Nyquist). All things being equal, this bandlimited version of the reflectivity is a good benchmark by which to compare our results, since it arguably represents the best that one could expect to obtain.

Figure 11 displays the (DC to half Nyquist passed) time-variant amplitude spectrum of the reflectivity estimate. Its conformity with the spectrum of the true reflectivity (Fig. 2) is quite remarkable.

Conclusions

A derivation, to first order, of a time-variant spectral model for the Gabor transform of a constant-Q-attenuated seismic trace was outlined. Using differential calculus and the calculus of variations, the model was fitted to the data in the least squares sense. This yielded estimates for Q and the seismic signature, and thus an estimate of the nonstationary, Q-attenuated wavelet. The theory was numerically evaluated via an algorithm for the Gabor deconvolution of a synthetic, Q-attenuated seismic trace. The illustrated example used an exceptionally low input Q-value, yet returned very promising initial deconvolution results. These favourable results, clearly reinforced by the fact that our model includes the convolutional model as a special case, strongly motivate further research in this direction.

Acknowledgements

References

Aki, K. and Richards, P. G., 1980, Quantitative seismology, theory and methods: W.H. Freeman and Company, Vol. 1 and 2.

Feichtinger, H. G. and Strohmer, T., 1998, Gabor analysis and algorithms, theory and applications: Birkhauser.

Gabor, D., 1946, Theory of communication: J. IEEE (London), 93, 429-457.

Grossman, J., Margrave, G.F., Lamoureux, M.P., and Aggarwala, R., 2001, Constant-Q wavelet estimation via a nonstationary Gabor spectral model: CREWES Research Report, Vol. 13.

Margrave, G. F., 1998, Theory of nonstationary linear filtering in the Fourier domain with application to time-variant filtering: Geophysics, **63**, 244-259.

Margrave, G. F. and Ferguson, R.J., 1998, Nonstationary filters, pseudodifferential operators, and their inverses: CREWES Research Report, Vol. 10.

Margrave, G. F. and Lamoureux, M.P., 2002, Gabor deconvolution: CSEG Convention expanded abstracts.

Marion, J. B., and Thornton, T. T., 1988, Classical dynamics of particles and systems: Harcourt Brace Jovanovich.

Sheriff, R. E. and Geldart, L. P., 1982, Data-processing and interpretation: Cambridge University Press, Vol. 2.

Figures
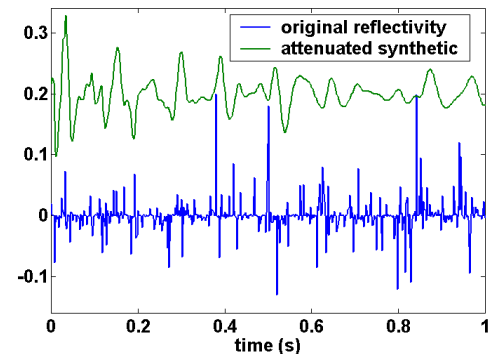
FIG. 1. A pseudo-random reflectivity (lower) and a nonstationary synthetic (upper) generated with an attenuation factor of 25.
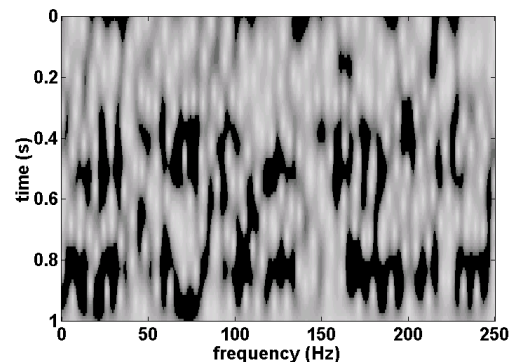
FIG. 2. Magnitude of the Gabor transform of the pseudo-random reflectivity of figure 1.
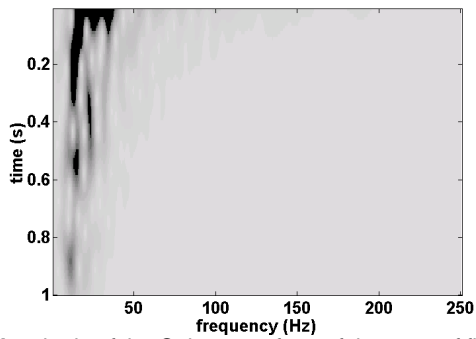
FIG. 3. Magnitude of the Gabor transform of the trace of figure 1.
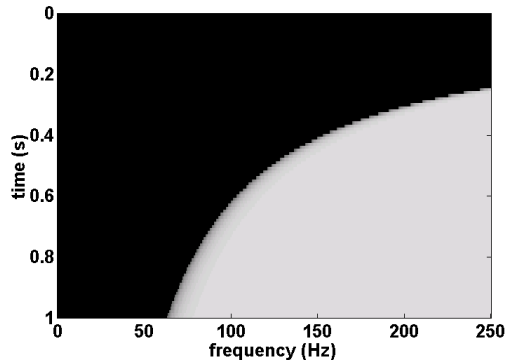
FIG. 4. Time-variant filter for weighting the Gabor spectrum of the synthetic trace according to the numerical precision of the data.
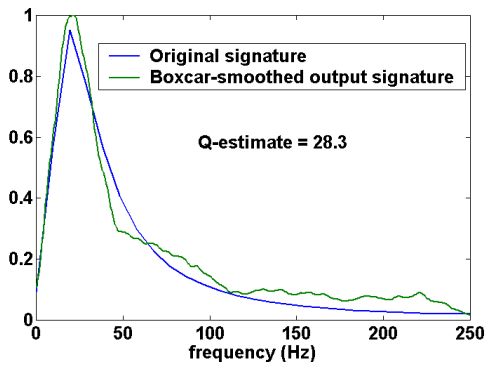
FIG. 5. Fourier amplitude spectra of the original and output seismic signatures. The output signature was smoothed with a boxcar to remove small residual oscillations.
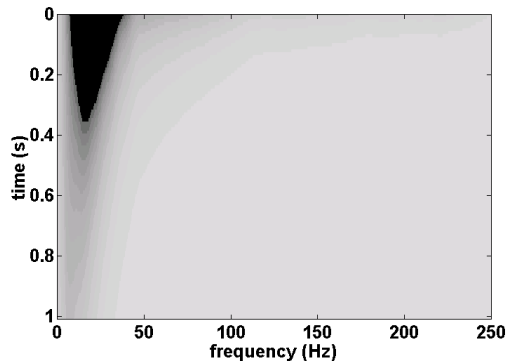
FIG. 6. The magnitude of the smoothed spectrum, which models the data in a least-squares sense. The point-wise inverse defines the magnitude of the deconvolution operator.
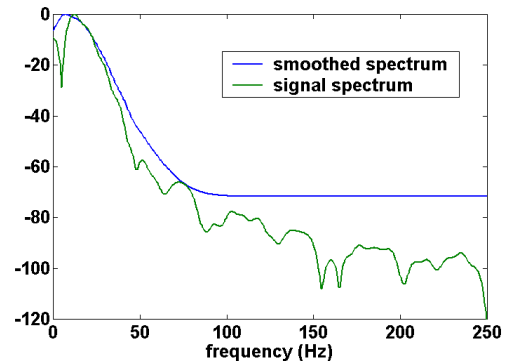
FIG. 7. Time slices of the input and least-squares-smoothed Gabor spectra at time t = 0.5s, plotted in decibels. A small stability constant was added to the smoothed Gabor spectrum to avoid division by excessively small numbers.
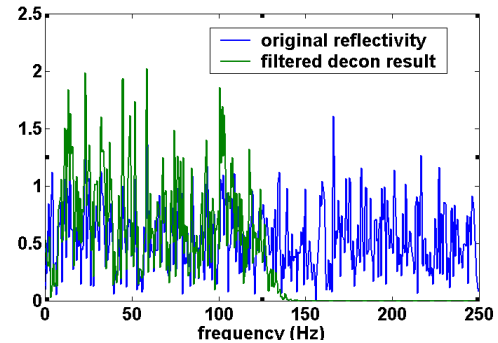
FIG.8. Fourier amplitude spectra of original reflectivity and Gabor deconvolution result.
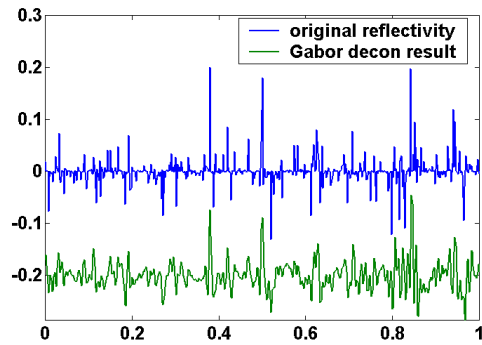
FIG. 9. The pseudo-random reflectivity of figure 1 (upper), and the bandpass-filtered Gabor deconvolution result (lower).
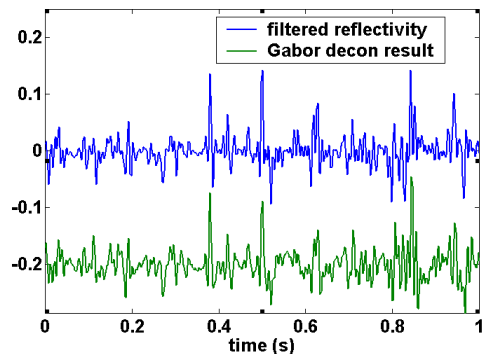
FIG. 10. Comparison of the bandpass-filtered Gabor deconvolution result (lower) with a bandpass-filtered (DC to half Nyquist) version of the reflectivity of figure 1 (upper).
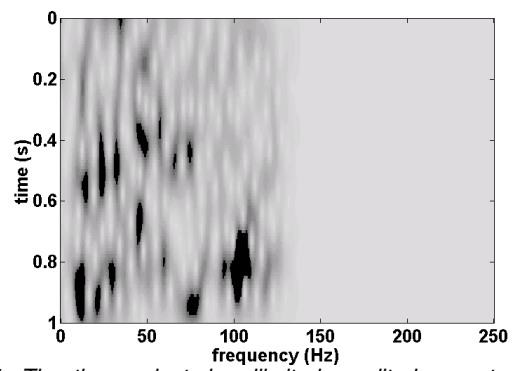
Fig. 11. The time-variant, bandlimited amplitude spectrum of the reflectivity estimate. Compare with the Gabor amplitude spectrum of the true reflectivity in figure 2.